Liquid Crystals
Publication details, including instructions for authors and subscription information:
http://www.informaworld.com/smpp/title~content=t713926090

Flow patterns and disclination-density measurements in sheared nematic liquid crystals I: Flow-aligning 5CB

P. T. Mather[ab]; D. S. Pearson[a]; R. G. Larson[c]
[a] Department of Materials, University of California, Santa Barbara, CA, U.S.A. [b] USAF Phillips Laboratory, Edwards AFB, CA, U.S.A. [c] AT&T Bell Laboratories, Murray Hill, NJ, U.S.A.

To cite this Article Mather, P. T. , Pearson, D. S. and Larson, R. G.(1996) 'Flow patterns and disclination-density measurements in sheared nematic liquid crystals I: Flow-aligning 5CB', Liquid Crystals, 20: 5, 527 — 538
To link to this Article: DOI: 10.1080/02678299608031139
URL: http://dx.doi.org/10.1080/02678299608031139

LIQUID CRYSTALS, 1996, VOL. 20, NO. 5, 527–538

Flow patterns and disclination-density measurements in sheared nematic liquid crystals I: Flow-aligning 5CB

by P. T. MATHER*†§, D. S. PEARSON†¶ and R. G. LARSON‡

† Department of Materials, University of California, Santa Barbara, CA 93106, U.S.A.

‡ AT&T Bell Laboratories, Murray Hill, NJ 07974-9636, U.S.A.

(*Received 26 October 1995; accepted 14 November 1995*)

We report the first direct measurements of disclination density during shear flow of a nematic liquid crystal. Samples of 4,4′-*n*-pentylcyanobiphenyl, or 5CB, are initially aligned in the homeotropic configuration within a torsional shear cell using surface treatment with lecithin. For low shearing rates, the director rotates within the shearing plane, except near the axis of rotation where irregular time-dependent out-of-plane orientation patterns exist. Disclinations form above a threshold shear rate, with the first 'thick' and 'thin' disclinations appearing near the sample edge, rapidly multiplying, and subsequently filling the sample. We measure the steady-state disclination density, ρ_A, the length of disclinations per unit projection area. The dimensionless disclination density, $\rho_A h$, where h is the sample thickness, is found to depend on two dimensionless quantities: Er, the Erickson number, *and* $\tilde{r}=r/h$, the scaled radial position. In the limit of large $\tilde{r}$ ($\tilde{r}>100$), the dependence of ρ_A on $\tilde{r}$ disappears and we find the empirical relation $\rho_A h \propto Er^{0.63}$.

1. Introduction

Nematic liquid crystalline materials in shear flow are known to exhibit disclination production [1, 2], leading to significant concentrations of disclination lines, mostly of strength $|S|=1$ ('thicks') or $|S|=\frac{1}{2}$ ('thins') [3]. It is generally believed that the presence of disclinations modifies the rheological behaviour [4] of liquid crystals or liquid crystalline polymers (LCPs), particularly the elasticity (storage modulus, normal stress differences, etc.) but also the viscosity (the so-called region I behaviour). The mechanism by which these material properties are affected by disclinations is largely unknown.

Although the 'threaded' texture has been observed for many years in flowing liquid crystals, a satisfactory understanding of disclination production in flow fields has remained elusive. One school of thought is that nematics of the *tumbling* type should be candidates for disclination production [4] because of their propensity for various flow instabilities [5]. Indeed, optical observations during shearing flow of tumbling nematics have shown production of disclinations [2, 6]. Here, *tumbling* refers to continual rotation of the director (i.e. the direction of average molecular orientation) with time. Most small-molecule nematics are of the *flow-aligning* type, however, which means that at steady state the director adopts a zero-viscous torque orientation within the shearing plane and close to the flow direction. The shearing plane is by definition parallel to both the flow direction and the velocity gradient direction. Surprisingly, initially aligned samples of the flow-aligning nematic *p*′-methoxybenzylidene-*p*-*n*-butylaniline, MBBA, have also been shown to produce disclinations during shear flow [1], making the connection between tumbling and disclination production unclear.

The goal of our research is to determine the correlation between tumbling and disclination production in shear flow by comparing the shear-flow behaviour of small-molecule nematics of similar chemical structure, but of differing sign of α_3, the Leslie viscosity indicating tumbling ($\alpha_3>0$) or flow-aligning ($\alpha_3<0$) behaviour. As a framework for their comparison, we monitor the director orientation using polarizing microscopy and measure the density of disclinations (projected length/area) present in each material under varying flow conditions. This paper will report the results of the flow-aligning nematic, 4,4′-*n*-pentylcyanobiphenyl (5CB) while a second paper in this series will report the results on the tumbling nematic, 4,4′-*n*-octylcyanobiphenyl (8CB).

2. Background

Experimental work on disclinations in sheared liquid crystals has necessarily employed light microscopy coupled with shearing capability. Graziano and Mackley [1]

* Author for correspondence.

§ Present address: USAF Phillips Laboratory, OLAC PL/RKFE, 10 E. Saturn Blvd., Edwards AFB, CA 93524-7680, U.S.A.

¶ Deceased.

0267-8292/96 $12·00

have made observations of MBBA in torsional shear flow and have catalogued many useful qualitative observations, particularly focusing on the susceptibility of disclination loops to deformation under viscous stress, as well as loop relaxation and contraction. 'Thicks', which are coreless (non-singular) defects of strength $|S| = 1$, and 'thins', which are singular defects of apparent strength $|S| = \frac{1}{2}$, were both observed. While 'thicks' nucleated from debris, 'thin' nucleation events were not observed within in the limited field of view and were assumed to be created at the edge of the cell from which they migrated toward the centre of the sample. It was also found, qualitatively, that the concentration of disclinations increased with increasing shear rate.

While experimentally challenging, some optical observations have also been made on thermotropic polymers in shear flow. Alderman and Mackley [7] and Graziano and Mackley [8] have observed shear flow of various thermotropic LCPs. Both studies have shown interesting textural transitions which occur upon increasing the frequency of oscillatory shear. It was found that the quiescent 'threaded texture', consisting of disclination loops, gave way to a 'line texture' when the sample was sheared at relatively low rates. This 'line texture' differs from the threaded texture in that it consists of finite, open lines flowing with the bulk material. Further increases in the oscillation frequency (shear rate) led to a more disordered 'worm texture', and then to a well-orientated material at the highest shear rate. Relaxation of the textures, which occurred over the tens of seconds, returned the sample to the threaded texture through the reverse progression of textures just described.

Similar studies were recently reported by DeNeve, Navard and Kleman [9, 10] who studied textural transitions in a commercially available thermotropic copolyesteramide, Vectra B950. *In-situ* observations were made using a rectilinear shear cell with microscopic observation capability, while *ex-situ* observations were made on sections microtomed from extrudates of a capillary rheometer. Quiescent and weakly sheared samples contained disclinations with strength, $|S| = 1/2$, and an increase in the shear rate led to a gradual transition from the worm texture to a well-oriented sample, the transition coinciding with the transition from a constant-viscosity plateau to a shear-thinning region of the flow curve [11]. They also observed damped oscillations in light transmitted through the worm texture and suggested that this is caused by alternating creation and annihilation of disclinations.

Theoretical work has addressed disclination behaviour in shear flow. Rey [12] has computed the behaviour of elastic loops, generated from the surfaces of a shear cell, in simple shear of a liquid with Newtonian rheological properties. Shear thickening or shear thinning is predicted, depending on the details of the calculation. Marrucci [13] has proposed a theory in which the defect lines are modeled as elastic dumbbells whose restoring force is a constant, independent of extension. But perhaps the most directly useful theoretical development is the scaling law proposed by Marrucci [4]. This scaling law postulates the existence of a material parameter, Er_{sat}, which is a limiting value of the texture-based Ericksen number, $Er_{tex} \propto \dot{\gamma} a^2$, where $\dot{\gamma}$ is the shear rate and a is a length scale characterizing the typical distance between disclinations. According to the scaling law, ER_{tex} saturates and remains constant with increasing applied shear rate during textural refinement [14]. A constant value of Er_{tex} implies that the density of disclinations increases with shear rate so that $a \propto \dot{\gamma}^{-1/2}$. While it is difficult to compare microscopic observations of disclinations with the defect dynamics theories on a quantitative basis, it is possible to check agreement with the notion of a limiting value of Er_{tex}.

3. Experimental

3.1 *Material*

5CB (4,4′-*n*-pentylcyanobiphenyl) was purchased from EM Industries and used as received. Sample purity was confirmed by clearing transition measurements which showed agreement with literature values to within 0·1°C. 5CB has the phase sequence: Cr 22·4°C N 34·5°C I. Experiments were conducted at 32·5°C ($T_{NI} - T = 2·0$°C).

3.2. *Rheological microscope*

For all our experiments, a custom 'rheological microscope' is used. A more detailed description of the apparatus is given elsewhere [15]. Figure 1 shows a schematic drawing of the apparatus. The flow geometry is torsional shear flow with vertical direction $\hat{y}$, the radial direction $\hat{r}$, and the azimuthal direction $\hat{\theta}$. The flow cell features two fused silica discs (*a*), 43 mm in diameter, with the bottom disc rotating relative to the top disc, creating a torsional flow field. The bottom disc is mounted to a rotary bearing table (*b*) (Master Machine Tools, Inc.) which features precision rotation. This rotary table is belt driven by a d.c. servo motor under velocity control (Rheometrics, Inc.). The top plate is separated from the bottom disc by manipulation with a kinematic mount (*c*) consisting of three micrometers, each with 0·5 μm resolution. The procedure used to set the sample thickness [15] yields thicknesses with accuracy ±2·5 μm.

For homeotropic (perpendicular) alignment of the samples, the disc surfaces are treated with lecithin in the usual manner [16].

To provide temperature control, two heat sources are used simultaneously. The primary heaters (*d*) [17] above and below the sample consist of foil heaters (aluminium

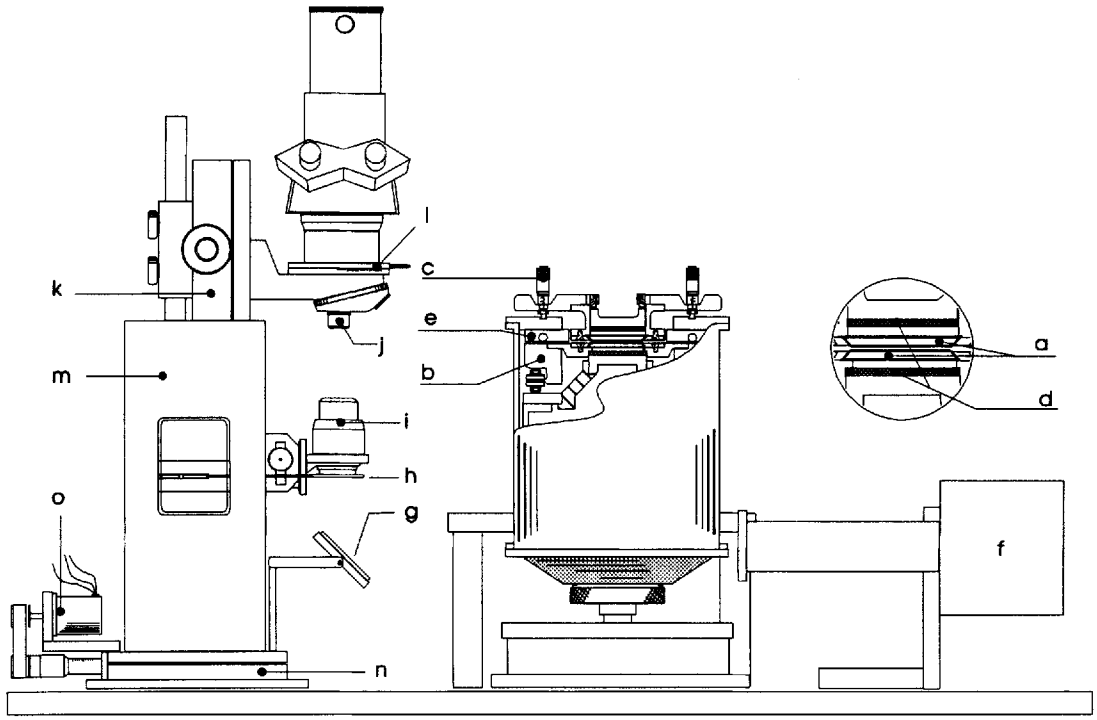

Figure 1. Schematic drawing of the apparatus: (*a*) fused silica discs, (*b*) rotary bearing table (Master Machine Tools, Inc.), (*c*) kinematic mount consisting of three micrometers, (*d*) foil heater assemblies (Heater Designs, Inc.) (*e*) guard heater using heating water from a circulation bath, (*f*) 50 W light source, (*g*) mirror, (*h*) polarizer, (*i*) condenser, (*j*) objective lens, (*k*) modular focus mount, (*l*) analyser, (*m*) microscope frame, (*n*) single axis translator, and (*o*) stepper motor for driving the translator.

etched on Kapton™), each sandwiched between a copper disc (cell side) and insulation. These heaters, connected electrically in parallel, receive power from a programmable power supply (Lambda LLS6018) under the control of a PID controller (Eurotherm 808) which senses the temperature near the centre of the sample using a J-type thermocouple. Heat loss near the cell edges is eliminated by using a guard heater (*e*) that completely surrounds the cell. This heater consists of a cylindrical aluminium block embedded with copper tubing through which thermostated silicon oil is flowed using a circulation bath (Fisher Scientific Isotemp — Model 9000). Use of both heating systems together provides temperature uniformity within the cell of better than $\pm 0{\cdot}1$°C.

The microscope optics are also shown in figure 1. The light source (*f*) is a 50 W tungsten lamp. The lamp beam is reflected upward through the optical path of the microscope by a mirror (*g*), is polarized with variable orientation (*h*) and then (optionally) condensed (*i*). Light transmitted through the sample is received by an objective lens (*j*) which is focused on the sample using the modular focus mount (*k*) capable of 1 μm positioning resolution. The light is next transmitted through an analyser of variable orientation (*l*), and passed to the eyepieces and to a CCD camera (Sony CCD-Iris, 768 × 493 pixels) or a still-photo camera (Nikon N8008).

The microscope, mounted on a frame (*m*), can be translated for viewing at different radial positions in the cell. For the torsional flow geometry, this allows observations at varying shear rate for a fixed rotation speed. This capability is automated by rotation of the translation stage micrometer (*n*) using a stepping motor (*o*). When operating the stepper motor at 200 steps revolution^{-1} the resulting radial position resolution is $\pm 1{\cdot}5$ μm.

For frame grabbing and image analysis, the CCD camera is sampled by an image processor (Matrox MVP-AT) residing in a PC-compatible computer. Raw video images are printed using a video printer (Polaroid Freeze-frame Video Printer).

As pointed out by Graziano and Mackley [1], the optical appearance of 'thick' and 'thin' disclinations can be made similar by transmitting light polarized perpendicular to the shear plane (vorticity direction) and observing with the analyser removed or parallel to the polarizer. The latter will be referred to as the 'vorticity configuration' and is the configuration used for the measurement of the disclination density. Another configuration, best for qualitative observation of disclinations in flow, transmits light polarized in the flow direction (analyser parallel to the polarizer) so that disclinations of differing strength may be distinguished.

Two objective lenses are used to measure disclination

density, depending on the vertical (y) resolution desired, y being the velocity-gradient direction. In most cases, we use a 5× objective lens with a depth of focus, d_f of approximately 750 μm, yielding a projected viewing of all disclinations across the cell gap for sample thicknesses, h, less than 750 μm. Alternatively, for vertical resolving power we use a 20× objective lens with a depth-of-focus of 4 ± 1 μm.

3.3. *Image processing*

Images containing disclinations are analysed to yield the length of disclination lines per unit projection area with no distinction between $|S| = 1$ and $|S| = \frac{1}{2}$ types. Due to the large contrast between the disclination lines with the background nematic, the images are readily reduced to binary images containing disclination pixels and background pixels using an intensity threshold. The set of disclination pixels is then 'dilated' and subsequently 'thinned' to yield sets of connected pixels, representing lines which are one pixel wide. The number of disclination pixels remaining following these steps is converted to the length of disclination lines, L, by using a μm/pixel calibration factor. Using the same calibration factor, the viewing area, A is calculated. Finally, the area-based disclination density, or length of lines per unit projection area, is calculated as $\rho_A = L/A$, a quantity equivalent to the integral of the disclination length per unit volume, ρ_V, integrated across the gap, $\rho_A = \int_0^h \rho_V(y)\mathrm{d}y$. Typical images resulting from the various stages of image processing are shown in figure 2.

To obtain an adequate signal-to-noise ratio in ρ_A measurements, approximately 1000 images must be analysed and the results averaged together. This requirement stems from the strongly fluctuating, turbulent, character of the disclination-filled texture in shear flow. A sample histogram of ρ_A, displayed in figure 3(*a*), shows the distribution of disclination densities for particular shear conditions (in this case for 8CB, but the nature of the distribution is similar for 5CB), which can be characterized by a Gaussian distribution with mean 15·33 mm^{-1} and standard deviation 5·03 mm^{-1}. Figure 3(*b*) is a plot of the raw disclination densities versus image number (dashed line) superposed with a plot of the cumulative average (solid) line.

A limit exists on the magnitude of the measurable disclination density. As the disclination density becomes large, the lines projected onto the viewing plane begin to cross frequently, leading to a disclination density measurement that is lower than the actual value. Additionally, when the spacing between lines becomes too small, the dilation step may bridge adjacent disclinations, leading again to an underestimation of the true disclination density. The relative effect of the above error sources is determined by the area fraction of the disclination lines following threshold, but prior to dilation and thinning. An estimation of the value of this area fraction

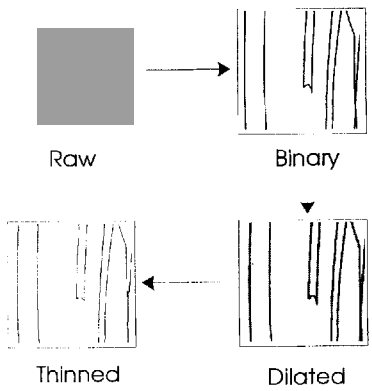

Figure 2. Example image processing sequence yielding contour lines which are one pixel wide, enabling extraction of disclination length within the field of view. Total disclination length is determined by 'skeletonizing' binary images (disclination pixel = 1, background = 0), summing the disclination pixels, and multiplying by the μm/pixel calibration factor.

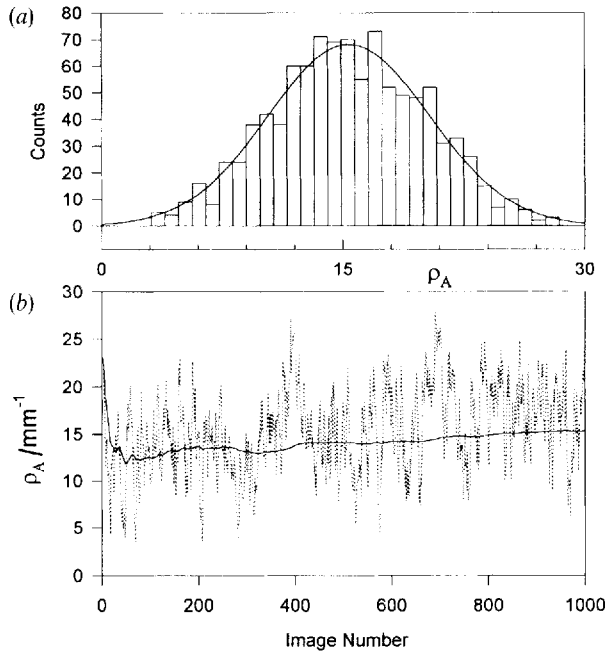

Figure 3. (*a*) Histogram of disclination density measured for a 250 μm sample of 8CB (qualitatively the same as for 5CB) for $Er = 1540$. The distribution is characterized by a Gaussian with mean 15·33 mm^{-1} and standard deviation 5·03 mm^{-1}. (*b*) Raw disclination density measurements versus image number (dashed line), used to construct the histogram (*a*), superposed with a plot of the cumulative average (solid line).

at which disclination density is significantly underestimated was made by measuring the average raw area fraction of disclination pixels as a function of increasing shear rate (which increases the disclination density) to the point where the measured disclination density saturated, showing significant deviation from the established trend with shear rate. From this method, it was concluded that the disclination density could be accurately measured for raw pixel area fractions less than 16·5 per cent.

The length of disclination lines, L, observed using an objective lens with a depth-of-focus, d_f, includes the contour length of disclinations within the field of view, projected on a horizontal (velocity-vorticity) plane, and summed over the depth of focus. Two regimes of interpretation exist with respect to the relative magnitude of d_f and the characteristic thickness, λ, of the disclination-containing zone of liquid in the gap [18]. For $d_f < \lambda$, the observed length, L, is proportional to the volumetric disclination density, ρ_V, calculated as $L/(Ad_f)$, where L is the observed length and A is the field of view. For $d_f > \lambda$, L is proportional to $\rho_A \equiv L/A$, here termed the area-based disclination density. Measurements of the distribution of ρ_V across the sample thickness utilize the 20× objective lens, for which $d_f < \lambda$.

4. Results and discussion

4.1. *Qualitative observations*

The response of 5CB to torsional shear flow was monitored using the various optical configurations discussed above as a function of increasing rotation speed, with the lowest obtainable rotation speed being 5×10^{-4} rad s^{-1}. For a typical sample thickness of 200 μm, this lowest speed corresponds to an Ericksen number at the cell edge of $Er_R \approx 10$, where the Ericksen number, Er is defined by $Er = (\gamma_1/K_3)\dot{\gamma}h^2$. Here, γ_1 is the twist viscosity, K_3 is the bend elastic constant, and $\dot{\gamma}$ is the shear rate. For 5CB at 32·5°C, the ratio of γ_1 to K_3 is approximately 7×10^{-5} s cm^{-2} [19, 20]. At low rotation speeds ($\dot{\theta} < 1 \times 10^{-2}$ rad s^{-1}, $Er_R < 200$), while viewing between crossed polarizers with monochromatic illumination, we observed the patterns of dark concentric rings superposed on a four-brush Maltese cross, as seen previously by Wahl and Fischer [21] and Skarp *et al.* [20]. The four-brush pattern arises from the fact that the director is oriented toward the flow direction within the plane of shear. Because the streamlines are circular, at two positions around the cell (for a given radius) the director is oriented in the polarizer direction, and at two other positions the director is oriented in the analyser direction. The positions are each separated by π/2. When the director is oriented in either the polarizer or analyser direction, the polarization of incident polarized light is not rotated by the birefringent sample and is therefore extinguished by the analyser, yielding the Maltese cross.

The rings, on the other hand, are a dramatic manifestation of the velocity field/director field coupling unique to liquid crystalline materials. Because the imposed shear rate, $\dot{\gamma} = r\dot{\theta}/h$, increases radially from zero at the centre, while the thickness is the same for all radial positions, the Ericksen number increases in proportion to the radial position. As a result, the average director orientation, which determines the retardation of light, increases radially. The radial increase in light retardation results in the concentric extinction ring patterns, each ring representing an order of birefringence. For example, the nth ring occurs at a radius where the retardation is $n\lambda_o$.

In figure 4(*a*), we show the four-brush pattern observed when the sample is viewed between crossed polarizers and illuminated, in this case, with white light. For this case, the sample thickness was 250 μm, and the rotation speed was 9×10^{-3} rad s^{-1} ($Er_R \approx 200$). With white light illumination, only the first few extinction

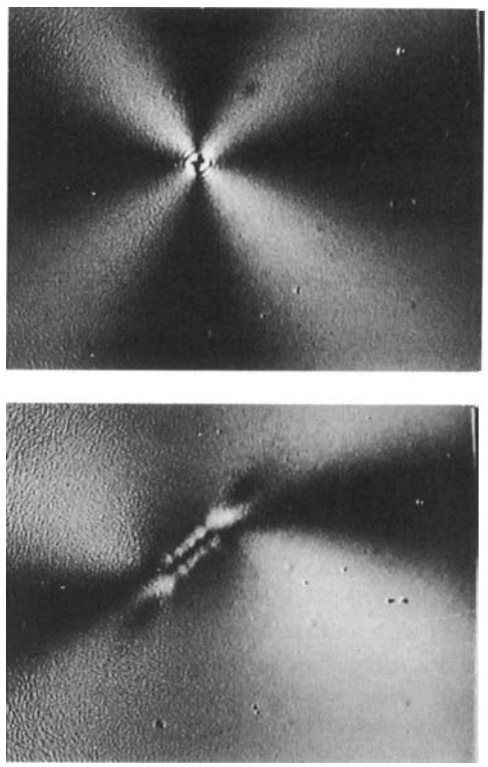

Figure 4. Example image of the centre of a 5CB cell when illuminated with white light. Rotation speed is 9×10^{-3} rad s^{-1}, thickness is 250 μm, and temperature is 32·5°C. The Maltese cross, whose arms are coincident with the directions of the polarizer (vertical) and analyser (horizontal), indicates that the director pattern is axisymmetric and, in this case, in the plane of shear (top). Squeezing fluctuation observed under the same conditions (bottom). The widths of these photomicrographs corresponds to a sample dimension of approximately 2 mm.

rings are visible very close to the sample centre, since the positions of higher order rings for different wavelengths begin to overlap. At this relatively high value of Er_R, bend elastic energy—from the director bending along the streamlines—is pumped into the system and the director orients progressively further toward the flow direction while remaining azimuthally oriented, due to the flow-aligning nature of the nematic. The process is similar to creating an $S=1$ disclination, with the disclination centred at the cell centre. Over time, the pattern of figure 4(*a*) transforms to one with time-dependent asymmetry with respect to the axis of rotation. A snapshot of this pattern at one instant is shown in figure 4(*b*). The time dependence features an exchange between three 'states', the exchange appearing rather random in time. The three states include the usual four brush pattern (see figure 4(*a*)), the two brush pattern shown in figure 4(*b*), and a pattern similar to figure 4(*b*), but with the two-brush pattern oriented vertically (rather than 'horizontally', as in figure 4(*b*)).

Above a rotation speed of 1×10^{-2} ($Er_R\approx225$), the ellipsoidal centre fluctuations concentrate to a type of disclination, or 'squeezing defect' which appears different from either $|S|=1$ ('thick') or $|S|=\frac{1}{2}$ ('thin') disclinations. The squeezing defect looks very similar to the structure in the centre of figure 4(*b*), but slightly longer and narrower. Short dark lines appear perpendicular to the long axis of the squeezing defect and evenly spaced along it. If the flow is stopped, these short dark lines begin to extend and eventually connect to form closed elliptically shaped rings. When the squeezing defect is present, the three-state time dependence ceases and only a two-brush pattern remains, with the brushes emanating from the ends of the squeezing defect. When the two-brush pattern is present, we find that by rotating the analyser relative to the polarizer (no longer crossed), a four-brush pattern can be regained. This implies that in two quadrants of the cell, the director is twisted in such a way that the extraordinary ray is adiabatically rotated with the director twist and the resultant emerging light is polarized with an orientation different than the analyser [22]. These effects are localized in the very centre of the cell and their effect on the director configuration throughout the cell could not be entirely investigated due to the limited viewing area available at the required magnification.

When viewing the entire region from the centre to the edge of the cell through the heater slit ('full slit-viewing'), where a macro lens is substituted for the objective lens, we found that these fluctuations in the centre have the effect of intermittently modifying the ring structure *globally* throughout the cell, but that the saturation of the director at the flow-alignment angle, within the plane containing the velocity and velocity gradient directions (shear plane)—observed indirectly by the divergence of the extinction ring spacing—remains. Based on these observations, it is not clear whether or not the appearance of the centre fluctuations and of the squeezing disclination have any other profound effects on the character of the flow. It was clear, however, that they are not the direct cause of disclination nucleation in the cell since it is not until much higher rotation speeds (*Er* values) that disclinations begin to appear.

Above $Er_R\approx4000$, disclinations are observed to fill the cell, first appearing *near* the edge and then spreading radially inward with time. It is not clear why this inward radial propagation occurs; however, we will show below that plots of disclination density versus shear rate (or *Er*) reveal tremendous hysteresis, with the disclination density measured during runs with decreasing *Er* remaining high even well below the threshold for disclination formation during runs with increasing *Er*. The observations of inward radial propagation of disclinations and disclination-density hysteresis are consistent with one another, as smaller radii correspond to smaller values of *Er*.

Disclinations of both 'thick' and 'thin' types are observed, with most thicks containing monopoles along their backbone. The behaviour of the disclinations in shear flow is very similar to that of MBBA as described by Graziano and Mackley [1]. In particular, we observe a wide range of disclination dynamics which alter the length of disclination lines. These include loop-contraction, loop-pinching, disclination-joining, and loop-stretching. Our observations of loop-pinching contradict an observation by Graziano and Mackley that disclinations are never seen to break apart or split open. While loop contraction is well understood [23], few accounts of the other length-altering events have been reported.

Figure 5 shows photomicrographs of disclinations observed in 5CB during shear flow with $Er=1500$ and $h=200\,\mu m$. Two thins are observed about to join (see figure 5(*a*), arrow). Such a lateral joining procedure is often followed by a vertical detachment, as shown schematically in figure 5(*b*). Two monopoles on a thick disclination line are shown acting as free joints in figure 5(*c*). This behaviour leads to 'pinching' in which a portion of the thick line pinches off and detaches as a free loop which ultimately contracts.

Nucleation of disclinations in the bulk during shear flow of 5CB is *never observed*. Therefore, in order to say where the disclinations are generated in 5CB, we must resort to explaining where they are *not* generated and then speculate as to most likely source. While no nucleation or loop birth is visible in the bulk, once disclinations somehow form, their length can change through stretching contraction, loop splitting, or recombination. This is

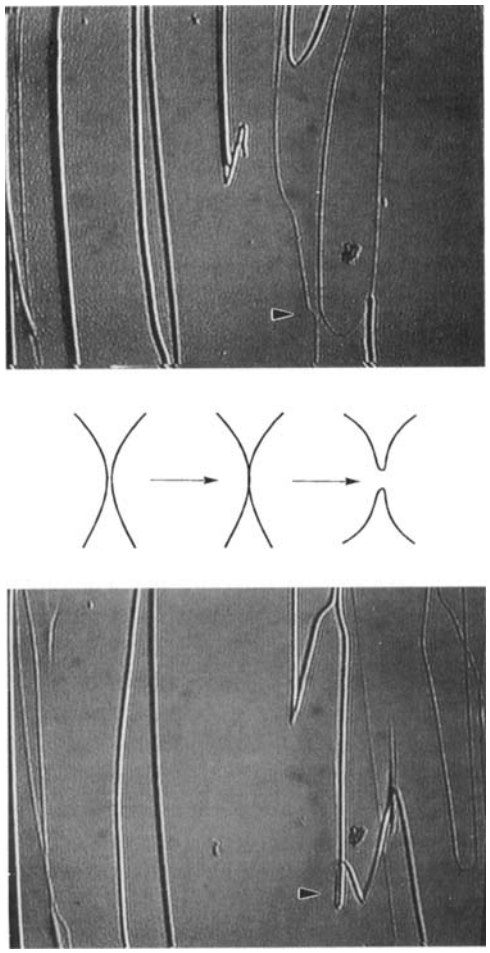

Figure 5. Photomicrographs of disclinations observed in 5CB during shear flow. $Er = 1500$ and $h = 200\,\mu m$. (*a*) Two thins are observed about to join (top photograph, arrow). (*b*) Schematic of exchange between two thin disclinations; laterally approaching disclinations meet and then detach vertically. (*c*) Two monopoles on a thick disclination line are shown acting as free joints (*c*) arrow. This behaviour leads to 'pinching' in which a portion of the thick line pinches off and detaches as a free loop which ultimately contracts. The width of this photomicrograph corresponds to a sample dimension of approximately 2 mm.

in contrast with the assumption made in Rey's model [12] that total length can only change by birth or annihilation of loops.

For MBBA in the same flow geometry, Graziano and Mackley reported that it was likely that $|S| = \frac{1}{2}$ disclination loops were created as the cell edge. Speculating that disclinations may form there due to a capillary instability or due to orientation effects at the nematic/air interface, we made long-duration observations at the cell edge during and after shear start-up. We did observe a small number of loop emission events, over the course of an hour. The mechanism of disclination formation at the edge appears to be the pinching of a pre-existing 'edge loop' caused by loop stretching in response to viscous drag. By edge loop, we refer to a small, $|S| = \frac{1}{2}$ disclination line which does not form a closed loop, but whose ends terminate at two points along a disc edge. Such an imperfection, while very rare, likely arises from incomplete lecithin (homeotropic aligning agent) coverage of the disc.

If edge nucleation were the only source of disclinations in the shear cell, some radial motion of the disclinations would be necessary to explain the distribution of disclinations throughout the cell that we see. To test this, we monitored the radial distribution of disclination density following the start of steady shearing, with $\dot{\theta} = 0{\cdot}25\,rad\,s^{-1}$ and $h = 225\,\mu m$ ($Er_R = 6600$), using the full slit-view optical set-up. The results are shown in figure 6, where photograph (*a*) was taken just after shear start-up ($t = 0^+$), (*b*) at $t = 120$ s, and (*c*) at 240 s. As can be seen by this photograph sequence, no obvious edge nucleation followed by radial motion is detected. Instead, we observe a gradual appearance of disclinations throughout the cell, with the density of scattering elements (possibly monopoles on the disclinations) increasing gradually with radius.

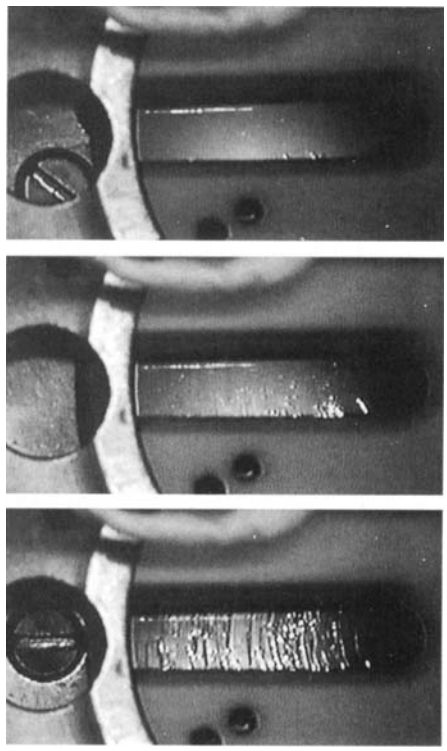

Figure 6. Full slit-view during shear start-up showing that the distribution of disclinations is not initially concentrated at the edge, but grows uniformly throughout the cell with time. Photograph times in seconds following shear start-up are (*a*) 0^+, (*b*) 120, and (*c*) 240. The slit width (vertical dimension) is 3·8 mm.

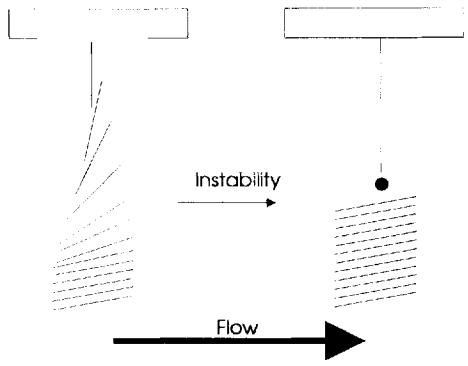

Figure 7. Schematic of a simple mechanism of disclination formation from the orientation boundary layer.

Although the disclinations in this optical configuration are barely visible and photograph poorly, it is clear that *edge nucleation cannot be the primary source of disclinations in the cell.* Since no bulk nucleation is observed either, only two possibilities remain: (i) loop nucleation in the bulk begins with infinitesimally small loops whose growth (increase in diameter) cannot be detected, or (ii) disclinations are being formed at the glass plate surfaces. It is also possible that a single disclination line, however formed, distorts the director and flow fields enough to lead to further disclination production in its vicinity, and thus to a multiplication of disclinations through the sample. We cannot conclude on the basis of our observations which case is predominant; however, the concept of an orientational surface boundary layer, which we now describe, lends support for (ii).

Flow-aligning nematics at high Ericksen number have a director profile which is uniform throughout most of the cell, the director being oriented at the flow-alignment angle ($\theta_{fa} = \tan^{-1}(\sqrt{(\alpha_3/\alpha_2)})$), except at the cell boundaries where the director reorients back to the prescribed boundary orientation over a distance, ζ, which is the boundary layer thickness. Pikin [24] has shown that this thickness decreases with Ericksen number as $\zeta = h(2/(Er^2 \cdot |\varepsilon|))^{1/4}$, where $\varepsilon = \alpha_3/\alpha_2$. Now, as the curvature of the director ($\partial^2\theta/\partial y^2$) is increased, the amount of stored elastic energy ($K \cdot \partial^2\theta/\partial y^2$) also increases. A region of large director curvature may be susceptible to an instability that lowers the distortional energy of the boundary layer at the expense of the energy required for defect creation. A simple schematic description of a mechanism for surface disclination nucleation is shown in figure 7 (where the surface is moving in the flow direction).

4.2. *Disclination density measurements*

The creation of disclinations in 5CB involves interesting hysteresis behaviour. When the rotation speed is ramped 'slowly' from rest, disclinations do not appear until a critical rotation speed (for a given sample thickness) is reached. Once this critical condition is met ($Er_R \approx 4000$) disclinations appear in large quantities, first near the cell edge, then quickly appearing at smaller and smaller radii. As mentioned previously, the observation that the cell fills radially with disclinations, when Er_R is gradually ramped from below a critical threshold, indicates that there is hysteresis, in that shear rates *lower* than the critical shear rate (edge shear rate at the transition) support disclinations. Further increase of the rotation speed gradually increases the disclination density at each radial position. When the rotation speed is decreased, the disclination density decreases, as expected, but significant numbers of disclinations remain even below the threshold observed during the previous ramp. Shown in figure 8 is disclination density, ρ_A, versus shear rate for increasing (●) and decreasing (○) shear rate, viewed near the cell edge. The plot displays a dramatic level of hysteresis, leading to the following two points.

First, the existence of a critical Er value for disclination formation may lend support for the surface nucleation hypothesis. To test this, an energy-based calculation is needed which determines the minimum Er for which the formation of a disclination is energetically favoured (i.e. distortional elasticity versus work-of-formation). This critical Er could then be compared with $Er \approx 4000$, the critical value we observe. Second, the hysteresis in disclination density suggests two possibilities regarding disclination nucleation. Either a substantial disclination nucleation rate is not critical in sustaining a substantial steady-state disclination density, or the critical Er for disclination nucleation is greatly lowered in the presence of disclination-modified flow. Since we never observe disclination nucleation, we favour the former possibility.

If the step-size of the rotation speed ($\Delta\dot{\theta}$) used in the ramp is increased, the critical shear rate for disclination creation is decreased as shown in the inset to figure 8. This suggests that the threshold for disclination formation is affected by the amplitude of the noise (transient director response to a step in shear rate). The rate of noise was not investigated further, but a systematic study would likely consist of superposition of random noise of varying amplitude on the motor control signal and observing the dependence of the transition point on the relative amplitude of the noise. The shape of the hysteresis exhibited in figure 8 is reminiscent of a sub-critical bifurcation [25].

To determine the distribution of disclination density across the sample thickness, the 20× objective lens was used to measure the volumetric disclination density, ρ_V, at positions finely spaced across the gap. Figure 9 shows the result of this experiment, for $Er = 5900$, $h = 400\,\mu m$,

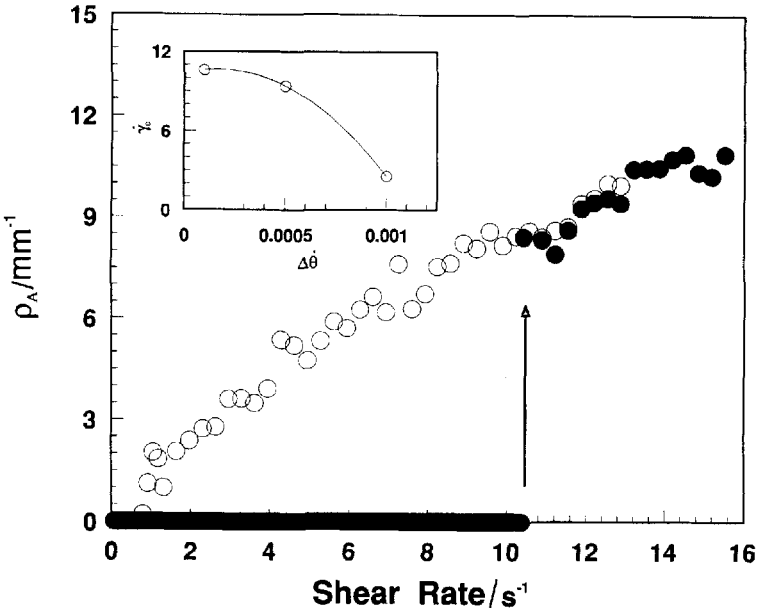

Figure 8. Hysteresis of scaled area-based disclination density in 5CB for $h=250\,\mu m$. Closed symbols are for rising shear rate and open symbols are for decreasing shear rate. The critical point corresponds to $Er\approx4100$. Increase of the rotation speed step-size leads to a decrease in the critical shear rate for disclination formation (inset).

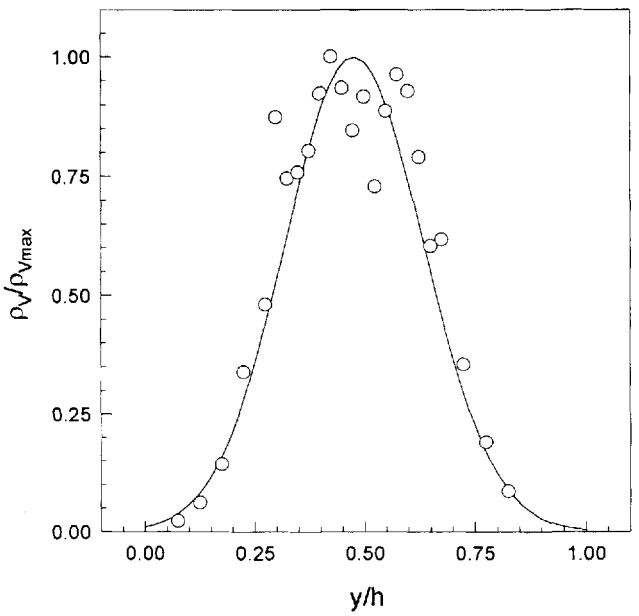

Figure 9. Distribution of the volumetric disclination density, ρ_V, across the sample thickness, normalized by maximum volumetric disclination density, ρ_{Vmax}. The sample thickness is 400 μm, $Er=5900$, and $\tilde{r}=40$. The solid line is a Gaussian fit to the data. The width-at-half-height of the distribution measures $0{\cdot}372\,h$.

and $\tilde{r}=40$, where $\tilde{r}=r/h$. The solid line represents a Gaussian fit to the data, with the width-at-half-height of the distribution being $0{\cdot}372\,h$. Under these conditions, then, disclination density is distributed symmetrically about the sample mid-plane. A possible explanation for this is that the disclinations are equally repelled by the two aligning surfaces. It is surprising, however, that the distribution is so narrow; measurements of the velocity profile would aid in the interpretation of this result.

We now present the results of a systematic investigation of the dependence of disclination density on shear rate and radial position. An example of the explicit dependence of disclination density on radius is shown in figure 10. Here, ρ_A is plotted versus shear rate where the data was obtained in two different ways, namely a radial sweep at a fixed rotation speed of $\dot{\theta}=0{\cdot}15\,rad\,s^{-1}$ (open symbols) and a rotation rate sweep at a fixed radius of 16·5 mm (filled symbols). It is evident from figure 10 that the disclination density is larger at smaller radial positions than would be the case if the shear rate were lowered at a constant radial position. *This suggests that a high curvature of streamlines tends to increase the density of disclinations.*

The effect of shear rate, radius, and gap thickness on disclination density can be represented empirically. The dimensional quantities in our experiments are the radial position (r), axial position (y), gap thickness (h), shear rate ($\dot{\gamma}$), and disclination density (ρ_A). From this set, along with material parameters, four dimensionless

quantities can be constructed: $\tilde{r}=r/h$, $\tilde{y}=y/h$, $Er=(\gamma_1/K_3)\dot{\gamma}h^2$, and $\tilde{\rho}_A=\rho_A h$. Here, Er represents the Ericksen number which, in the usual sense, is a measure of the relative influence of hydrodynamic and elastic stresses. In defining Er, we choose the twist viscosity ($\gamma_1=\alpha_3+|\alpha_2|$) and the bend elastic constant K_3. The bend elastic constant is used because deviations of the director from the homeotropic boundary conditions are met with resistance due to bend elastic torque. Since all experiments were performed at fixed temperature, where the material constants are fixed, the appropriateness of the choices of constants is not tested. Other choices would yield an Ericksen number of the same order of magnitude.

Given this simple dimensional analysis, one expects the general relationship:

$$\tilde{\rho}_A=f(Er,\tilde{r}). \tag{1}$$

Recall that in the measurement of ρ_A, the axial position, y, is effectively averaged over and therefore $\tilde{y}$ does not appear in equation (1). Thus, the dimensional analysis implies that plots of $\tilde{\rho}_A$ versus Er should superpose for fixed $\tilde{r}$.

Example scaled data appear in figure 11 and 12 for $\tilde{r}=30$ and 40, respectively, where data from three thicknesses 250 (●), 300 (○), and 400 (◇) μm are plotted. Superposition of data for fixed $\tilde{r}$ is observed. Also, a power law dependence (solid lines) of ρ_A on Er emerges with the parameters of the power law containing the dependence of ρ_A on $\tilde{r}$.

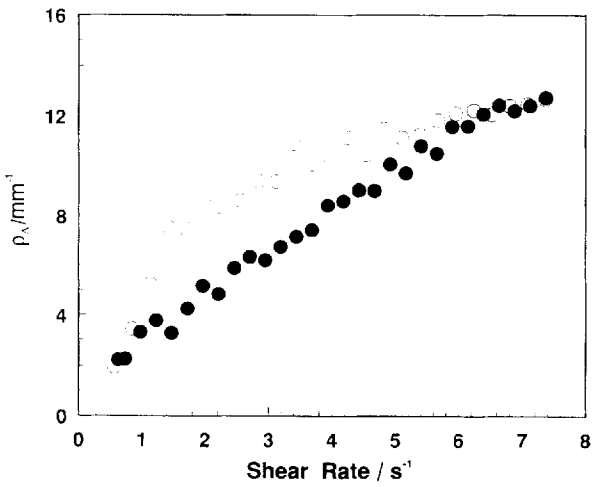

Figure 10. Disclination density ρ_A versus shear rate for 5CB obtained using a radial sweep (open symbols) at fixed rotation speed (0·15 rad s^{-1}) and with a rotation speed sweep at fixed radial position of 16·5 mm. Sample thickness is 335 μm.

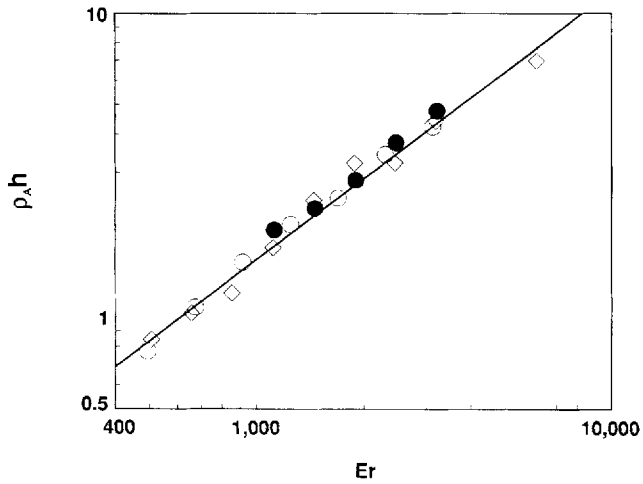

Figure 11. Dimensionless disclination density $\rho_A h$ versus Er for 5CB at 32·5°C and $\tilde{r}=30$ for gap thicknesses of 250 μm (○), 300 μm (●), and 400 μm (◇). The solid line represents a power law fit to the 400 μm data.

Power law fits were performed on data from samples of four thicknesses: 150, 250, 300 and 400 μm, and with $\tilde{r}$ ranging from 14 to 117. With the power-law expressed as

$$\rho_A h=\alpha(\tilde{r})Er^{\beta(\tilde{r})}, \tag{2}$$

the dependence of α (filled symbols) and β (open symbols) on $\tilde{r}$ is shown in figure 13. From this figure, one can identify three regions within the torsional shear cell: (I) the inner region, $\tilde{r}<20$, within which disclination density is negligible, (II) a transition region $20<\tilde{r}<70$, where the dependence of disclination density on $\tilde{r}$ is greatest, and (III) an outer or 'local scaling' region, $\tilde{r}>90$, where

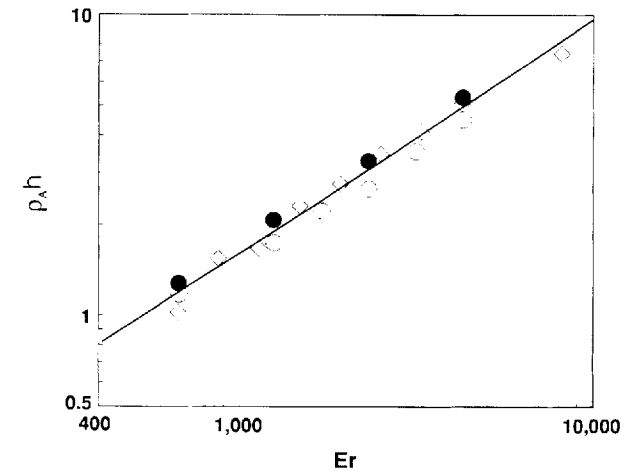

Figure 12. Dimensionless disclination density $\rho_A h$ versus Er for 5CB at 32·5°C and $\tilde{r}=40$ for gap thicknesses of 250 μm (○), 300 μm (●), and 400 μm (◇). The solid line represents a power law fit to the 400 μm data.

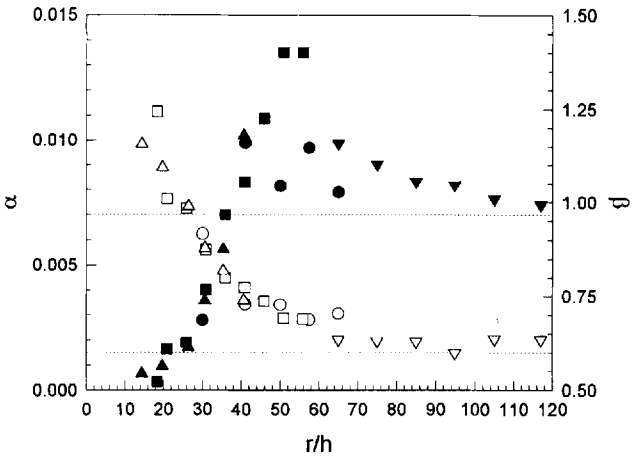

Figure 13. Dependence of power law parameters, α (filled symbols) and β (open symbols), on $\tilde{r}=r/h$ for 150 μm (▽), 250 μm (○), 300 μm (□), and 400 μm (△).

disclination density depends only on Er. In the local scaling regime, region (III), we find that

$$\lim_{\tilde{r}\to\infty}\alpha = 7{\cdot}5\times10^{-3}\ \text{mm}^{-1} \text{ and } \lim_{\tilde{r}\to\infty}\beta = 0{\cdot}635.$$

The dependence of disclination density on the dimensionless radial coordinate for $\tilde{r}<90$ probably reflects an influence of the curvature of the streamlines, though it is difficult to provide a detailed explanation of the form of this dependence.

It is significant that the value of β in the limit of large $\tilde{r}$ is different from that predicted by the Marrucci scaling law [4], which gives $\beta=1/2$. This difference suggests that there exists more underlying physics than the simple balance of elastic and viscous stresses, as proposed by Marrucci, in determining the density of disclinations. Other, indirect, measurements of texture length scale in sheared LCPs have also found deviation from $\beta=\frac{1}{2}$ [26].

6. Summary

During shear flow of 5CB, the director was found to stay within the shear plane for all Er (prior to disclination formation) except near the centre of the torsional shear cell. No disclination nucleation events were directly observed, except for infrequent 'loop-pinching' events spawned from pre-existing loops near the cell edge. These few edge nucleation events were determined *not* to be the primary source of disclinations in the shear cell, since observation of the cell as a whole following shear start-up showed disclinations appearing at a rate which was radially uniform; i.e. disclinations do not fill the cell via edge nucleation followed by inward radial motion. We hypothesize that disclinations are nucleated from the boundary layers, where the director is distorted over short length scales for large Er. The large hysteresis in disclination density versus Er suggests that nucleation events in 5CB are relatively unimportant in determining the density of disclinations at steady state, although the disclination nucleation rate may play a critical role in transient disclination density following shear start-up, for example.

The disclination density, ρ_A = length/projection area, was measured as a function of Er and $\tilde{r}=r/h$, where h is the sample thickness. We found that plots of the scaled disclination density, $\rho_A h$, versus Er show power law behaviour of the form, $\rho_A h=\alpha Er^{\beta}$. The power law parameters, α and β, depend on $\tilde{r}$, except for $\tilde{r}>90$. The scaling exponent, β, was found to be 0·635 for $\tilde{r}>90$, in disagreement with the prediction of $\beta=0{\cdot}5$ from the dimensional scaling theory of Marrucci.

The authors would like to thank Mohan Srinivasarao and Mike Dennin for several enlightening discussions.

References

[1] Graziano, D. J., and Mackley, M. R., 1984, *Mol. Cryst. liq. Cryst.*, **106,** 103.
[2] Cladis, P. E., and Torza, S., 1976, *Colloid. Interface Sci.*, **4,** 487.
[3] See for example, Kleman, M., 1991, *Liquid Crystallinity in Polymers: Principles and Fundamental Properties*, edited by Alberto Cifferri (VCH Publishers, Inc.) Chap. 10.
[4] Marrucci, G., and Greco, F., 1993, *Adv. Chem. Phys.*, **86,** edited by I. Prigogine and Stuart Rice (New York: Wiley Publishers.)
[5] Dubois-Violette, E., Durand, G., Guyon, E., Manneville, P., and Pieranski, P., 1978, *Solid State Phys. Suppl.*, **14,** 147.
[6] Gähwiller, C., 1972, *Phys. Rev. Lett.*, **28,** 1554.
[7] Alderman, N. J., and Mackley, M. R., 1985, *Faraday Discuss. Chem. Soc.*, **79,** 149.
[8] Graziano, D. J., and Mackley, M. R., 1984, *Mol. Cryst. liq. Cryst.*, **106,** 73.
[9] DeNeve, T., Kleman, M., and Navard, P., 1992, *J. Phys. II. France*, **2,** 187.
[10] DeNeve, T., Navard, P., and Kleman, M., 1993, *J. Rheol.*, **37,** 515.
[11] Here, we refer to the typical three region flow curve observed for many LCPs in which plots of steady shear viscosity versus shear rate feature shear thinning at the lowest rates (region I), a Newtonian plateau at intermediate rates (region II), and shear thinning again at the highest rates (region III).
[12] Rey, A., 1993, *Mol. Cryst. liq. Cryst.*, **225,** 313.
[13] Marrucci, G., and Maffettone, P. L., 1993, *International Workshop on Liquid Crystalline Polymers*, edited by C. Carfagna (Tarrytown, NY: Pergamon Press).
[14] Burghadt, W. R., and Fuller, G. G., 1990, *J. Rheol.*, **34,** 959.
[15] Mather, P. T., 1994, PhD Dissertation, U. C. Santa Barbara, USA.
[16] Cognard, J., 1982, *Mol. Cryst. liq. Cryst.*, **S1.**
[17] This heater design was kindly suggested by Dr M. Mackley.

[18] $\bar{\lambda}$ is less than the sample thickness, h, because disclinations tend to be excluded from the boundary layer near the glass surfaces.
[19] KARAT, P. P., and MADHUSUDANA, N. V., 1976, *Mol. Cryst. liq. Cryst.*, **36,** 51.
[20] SKARP, K., LAGERWALL, S. T., and STEBLER, B., 1980, *Mol. Cryst. liq. Cryst.*, **60,** 215.
[21] WAHL, J., and FISCHER, F., 1973, *Mol. Cryst. liq. Cryst.*, **22,** 359.
[22] SRINIVASARAO, M., 1992, private communcation.
[23] See for example DEGENNES, P. G., 1973, *Molecular Fluids*, edited by R. Balian and G. Weill (New York: Gordon and Breach Science Publishers.)
[24] PIKIN, S. A., 1974, *Soviet Phys. JETP*, **38,** 1246.
[25] DRAZIN, P. G., and REID, W. H., 1981, *Hydrodynamic Stability* (New York: Cambridge University Press).
[26] BURGHARDT, W. R., and HONGLADAROM, K., 1994, *Macromolecules*, **27,** 2327.